Journal of the Faculty of Environmental Science and Technology, Okayama University
Vol. 1, No. 1, pp.121-133, March 1996

Numerical Analysis of Dynamic Behavior of Highly Saturated Sand Bed around Cylindrical Block under Cyclic Loading of Water Pressure

Shiro MAENO*, Tetsuo YAMAMOTO, Hiroshi NAGO***

(Received January 16 , 1996)

In this paper the theoretical procedure to analyze the dynamic behavior of highly saturated sand bed around a cylindrical block under the cyclic loading of water pressure is developed. The fundamental equations were derived for the axially symmetric coordinates. Then, the finite element equations were developed to solve these fundamental equations numerically. Finally, the numerical method was verified by experiments.

1. INTRODUCTION

Many types of collapse of coastal structures occurs under stormy waves. One of them is the settlement of armour blocks used for the protection of coastal structures such as breakwater. To understand the mechanism of this settlement phenomenon we have investigated the settlement of a rectangular parallelepiped block on the sand bed under the cyclic loading of water pressure both experimentally and theoretically[1),2)]. The settlement of concrete block and the characteristics of the sand movement around the block were made clear by the experiment. And it is also clarified that the cyclic seepage force which occurs around the block under water pressure variation plays an important role to the settlement phenomenon. To get pore water pressure distribution around the block in detail, we derived the fundamental equations to analyze the dynamic behavior of the sand bed and carried out the vertical two-dimensional finite element analysis[3),4)]. The validity of numerical analysis was verified by comparing with the experimental results. For the analysis the plain strain state was assumed in consideration of the experimental conditions.

Photo 1 shows one of the experimental results. The colored sand and the standard sand next to the front side wall of the container get mixed. It can be noticed that the effect of the front and the back side walls of the container appears. As long as assuming the plane strain state and using a rectangular parallelepiped block as a sinking object for the experiment, the wall effect can

*Department of Environmental and Civil Engineering, **Graduate student of Okayama Univ.

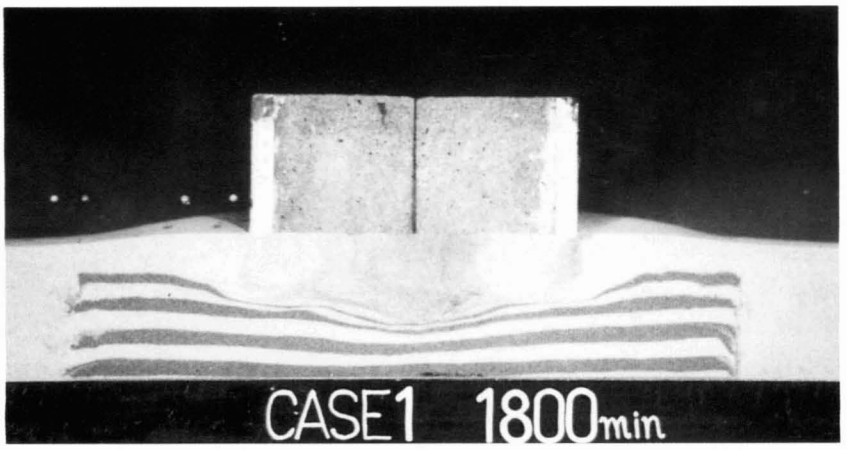

Photo 1 Experiments for rectangular block

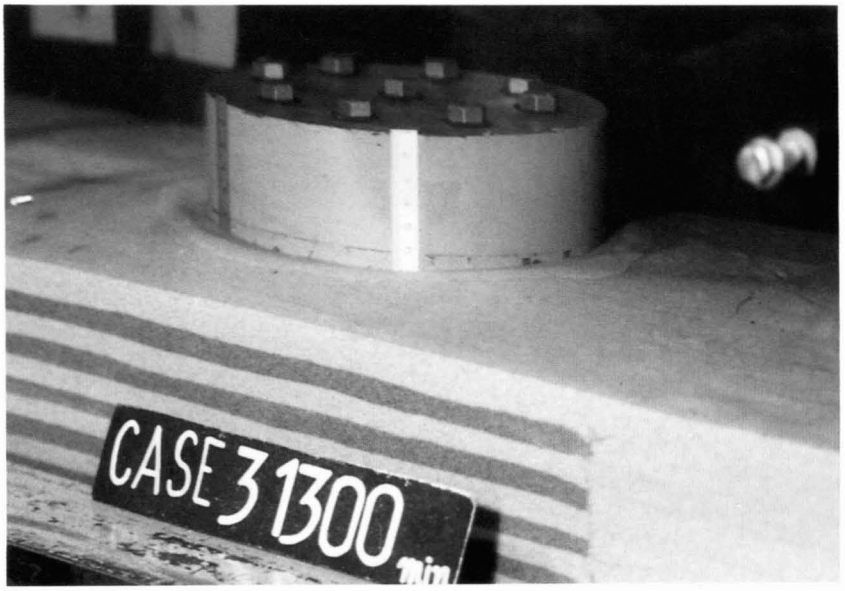

Photo 2 Experiments for cylindrical block

not be neglected. To reduce this effect, we used a cylindrical block as a sinking object for the experiment as shown in Photo 2. Very little effect of the side walls of the container is seen in this photo. To get more information about the dynamic behavior of the sand bed around a cylindrical block under the cyclic loading of water pressure, it is necessary to develop a mathematical model to explain the phenomenon.

In this study, from the above point of view, we first derived the fundamental equations to analyze the dynamic behavior of the sand bed around the block for the axially symmetric coordinates. Then, the finite element equations were derived to solve the fundamental equations numerically. Finally, the validity of this numerical method was verified by the experiment.

2. FUNDAMENTAL EQUATIONS

2.1 Fundamental Equations for Cartesian Coordinates

In the theoretical treatment, following fundamental assumptions are adopted.

(1) The sand layer and the water are compressible.

(2) The pore water moves in accordance with Darcy's law.

(3) The skeleton of the sand layer deforms in accordance with Hooke's law.

(4) The sand layer is composed of three phases ; sand, water and air. Then, the porosity λ is the sum of the part for the water λ_w and the part of the air λ_a. That is,

$$\lambda = \lambda_w + \lambda_a \tag{1}$$

Under these assumptions we derived fundamental equations in Cartesian coordinates as follows[3),5)]. Taking into account the pore water pressure p, equilibrium conditions are expressed by the following equations.

$$\left.\begin{aligned} \frac{\partial \sigma_x}{\partial x} + \frac{\partial \tau_{yx}}{\partial y} + \frac{\partial \tau_{zx}}{\partial z} &= \frac{\partial p}{\partial x} \\ \frac{\partial \tau_{xy}}{\partial x} + \frac{\partial \sigma_y}{\partial y} + \frac{\partial \tau_{zy}}{\partial z} &= \frac{\partial p}{\partial y} \\ \frac{\partial \tau_{xz}}{\partial x} + \frac{\partial \tau_{yz}}{\partial y} + \frac{\partial \sigma_z}{\partial z} &= \frac{\partial p}{\partial z} \end{aligned}\right\} \tag{2}$$

where, $\sigma_x, \sigma_y, \sigma_z$ are incremental normal stresses (deviations from the initial stress state), and $\tau_{xy}, \tau_{yz}, \tau_{zx}$ are incremental shear stresses. These stress components are expressed by the following stress-strain relationship.

$$\left.\begin{aligned} \sigma_x &= 2G\varepsilon_x + \lambda' e, \quad \tau_{xy} = \tau_{yx} = G\gamma_{xy} \\ \sigma_y &= 2G\varepsilon_y + \lambda' e, \quad \tau_{yz} = \tau_{zy} = G\gamma_{yz} \\ \sigma_z &= 2G\varepsilon_z + \lambda' e, \quad \tau_{zx} = \tau_{xz} = G\gamma_{zx} \end{aligned}\right\} \tag{3}$$

where, λ' is Lame's constant. G is the shear modulus. They are given by the following relation.

$$\lambda' = \frac{\nu E}{(1+\nu)(1-2\nu)}, \quad G = \frac{E}{2(1+\nu)} \tag{4}$$

(ν : Poisson's ratio, E : Young's modulus)

$\varepsilon_x, \varepsilon_y, \varepsilon_z$ and $\gamma_{xy}, \gamma_{yz}, \gamma_{zx}$ re components of incremental strains. e is the incremental volumetric strain according to the following relation.

$$e = \varepsilon_x + \varepsilon_y + \varepsilon_z \tag{5}$$

The strains are related to the displacements by the following expressions in case of small deformation.

$$\left.\begin{aligned} \varepsilon_x &= \partial u_x / \partial x, \quad \gamma_{xy} = \partial u_x / \partial y + \partial u_y / \partial x \\ \varepsilon_y &= \partial u_y / \partial y, \quad \gamma_{yz} = \partial u_y / \partial z + \partial u_z / \partial y \\ \varepsilon_z &= \partial u_z / \partial z, \quad \gamma_{zx} = \partial u_z / \partial x + \partial u_x / \partial z \end{aligned}\right\} \tag{6}$$

where, u_x, u_y, u_z are displacement components in x, y, z directions respectively.
On the other hand, the continuity equation for pore water is[3)]

$$(\beta\lambda_w + \frac{\lambda_a}{P})\frac{\partial p}{\partial t} + \frac{\partial e}{\partial t} = (\frac{k}{\rho_w g})\nabla^2 p \tag{7}$$

where, k :permeability coefficient, ρ_w : density of the pore water, g : acceleration due to gravity, t : time, β : compressibility of the water, P : absolute pressure, ∇^2 is vector operation defined by

$$\nabla^2 = \frac{\partial^2}{\partial x^2} + \frac{\partial^2}{\partial y^2} + \frac{\partial^2}{\partial z^2} \tag{8}$$

2.2 Fundamental Equations for Axially Symmetric Coordinates

In Fig. 1 an cylindrical element is drawn together with stress components acting on the surface of the element. Performing coordinates transformation of equilibrium equations (2) for Cartesian coordinates, following equilibrium equations for cylindrical coordinates are obtained[5),6)].

$$\left.\begin{aligned} \frac{\partial \sigma_r}{\partial r} + \frac{1}{r}\frac{\partial \tau_{\theta r}}{\partial \theta} + \frac{\partial \tau_{zr}}{\partial z} + \frac{\sigma_r - \sigma_\theta}{r} &= \frac{\partial p}{\partial r} \\ \frac{\partial \tau_{r\theta}}{\partial r} + \frac{1}{r}\frac{\partial \sigma_\theta}{\partial \theta} + \frac{\partial \tau_{z\theta}}{\partial z} + \frac{2\tau_{r\theta}}{r} &= \frac{1}{r}\frac{\partial p}{\partial \theta} \\ \frac{\partial \tau_{rz}}{\partial r} + \frac{1}{r}\frac{\partial \tau_{\theta z}}{\partial \theta} + \frac{\partial \sigma_z}{\partial z} + \frac{\tau_{rz}}{r} &= \frac{\partial p}{\partial z} \end{aligned}\right\} \tag{9}$$

$\sigma_r, \sigma_\theta, \sigma_z$ are stresses in r, θ, z directions respectively. $\tau_{r\theta}, \tau_{\theta z}, \tau_{zr}$ are shear stresses. The stress components are expressed by the following stress-strain relationship.

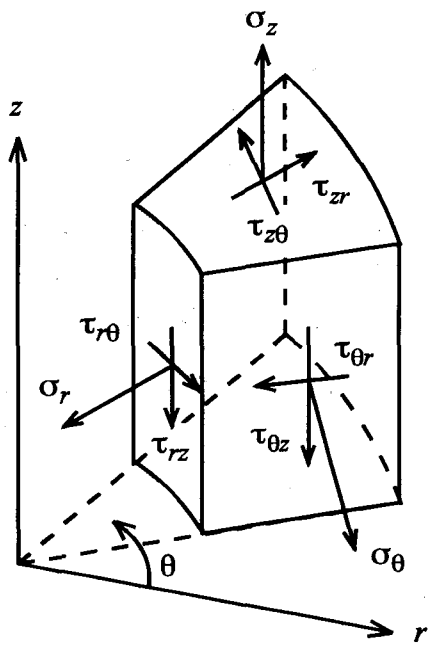

Fig. 1 Stress components in cylindrical coordinates

$$\left.\begin{aligned} \sigma_r &= 2G\varepsilon_r + \lambda' e, \quad \tau_{r\theta} = \tau_{\theta r} = G\gamma_{r\theta} \\ \sigma_\theta &= 2G\varepsilon_\theta + \lambda' e, \quad \tau_{\theta z} = \tau_{z\theta} = G\gamma_{\theta z} \\ \sigma_z &= 2G\varepsilon_z + \lambda' e, \quad \tau_{zr} = \tau_{rz} = G\gamma_{zr} \end{aligned}\right\} \tag{10}$$

$$e = \varepsilon_r + \varepsilon_\theta + \varepsilon_z \tag{11}$$

These equations are equivalent to Eqs. (3) and (5). The strain components are defined as follows.

$$\left.\begin{aligned} \varepsilon_r &= \frac{\partial u_r}{\partial r}, & \gamma_{r\theta} &= \frac{1}{r}\frac{\partial u_r}{\partial \theta} + \frac{\partial u_\theta}{\partial r} - \frac{u_\theta}{r} \\ \varepsilon_\theta &= \frac{1}{r}\frac{\partial u_\theta}{\partial \theta} + \frac{u_r}{r}, & \gamma_{\theta z} &= \frac{\partial u_\theta}{\partial z} + \frac{1}{r}\frac{\partial u_z}{\partial \theta} \\ \varepsilon_z &= \frac{\partial u_z}{\partial z}, & \gamma_{zr} &= \frac{\partial u_z}{\partial r} + \frac{\partial u_r}{\partial z} \end{aligned}\right\} \tag{12}$$

where, u_r, u_θ, u_z are displacement components in r, θ, z directions respectively.

In cylindrical coordinates system, the vector operation in Eq. (8) becomes

$$\nabla^2 = \frac{1}{r}\frac{\partial}{\partial r}\left(r\frac{\partial}{\partial r}\right) + \frac{1}{r^2}\frac{\partial^2}{\partial \theta^2} + \frac{\partial^2}{\partial z^2} \tag{13}$$

As shown in Photo 2, the dynamic behavior of the sand bed around the cylindrical block under the cyclic loading of water pressure can be treated as an axially symmetric problem. In case of axially symmetric problem, following conditions exist.

$$u_\theta = 0, \quad \partial u_r / \partial \theta = 0, \quad \partial u_z / \partial \theta = 0, \quad \partial p / \partial \theta = 0 \tag{14}$$

Using these conditions, relationship (9) is reduced to

$$\left.\begin{aligned} \frac{1}{r}\frac{\partial}{\partial r}(r\sigma_r) + \frac{\partial \tau_{zr}}{\partial z} - \frac{\sigma_\theta}{r} &= \frac{\partial p}{\partial r} \\ \frac{1}{r}\frac{\partial}{\partial r}(r\tau_{rz}) + \frac{\partial \sigma_z}{\partial z} &= \frac{\partial p}{\partial z} \end{aligned}\right\} \tag{15}$$

Eqs. (10), (11) and (12) are reduced to

$$\left.\begin{aligned} \sigma_r &= 2G\varepsilon_r + \lambda' e, & \tau_{r\theta} &= \tau_{\theta r} = 0 \\ \sigma_\theta &= 2G\varepsilon_\theta + \lambda' e, & \tau_{\theta z} &= \tau_{z\theta} = 0 \\ \sigma_z &= 2G\varepsilon_z + \lambda' e, & \tau_{zr} &= \tau_{rz} = G\gamma_{zr} \end{aligned}\right\} \tag{16}$$

$$e = \partial u_r / \partial r + u_r / r + \partial u_z / \partial z \tag{17}$$

$$\left.\begin{aligned} \varepsilon_r &= \frac{\partial u_r}{\partial r}, & \gamma_{r\theta} &= 0 \\ \varepsilon_\theta &= \frac{u_r}{r}, & \gamma_{\theta z} &= 0 \\ \varepsilon_z &= \frac{\partial u_z}{\partial z}, & \gamma_{zr} &= \frac{\partial u_z}{\partial r} + \frac{\partial u_r}{\partial z} \end{aligned}\right\} \tag{18}$$

And the vector operation (13) is reduced to

$$\nabla^2 = \frac{1}{r}\frac{\partial}{\partial r}\left(r\frac{\partial}{\partial r}\right) + \frac{\partial^2}{\partial z^2} \tag{19}$$

Then the continuity equation expressed as

$$(\beta\lambda_w + \frac{\lambda_a}{P})\frac{\partial p}{\partial t} + \frac{\partial e}{\partial t} = (\frac{k}{\rho_w g})\left(\frac{1}{r}\frac{\partial}{\partial r}(r\frac{\partial p}{\partial r}) + \frac{\partial^2 p}{\partial z^2}\right) \tag{20}$$

Eq. (15) and Eq. (20) are the fundamental system of equations to analyze the dynamic behavior of sand bed around the cylindrical block. There are three unknown quantities in these equations. Two of them are incremental displacements u_r and u_z. Another one is incremental pore water pressure p. Consequently the governing equations are written as follows.

$$\frac{1}{r}\frac{\partial}{\partial r}(r\sigma_r) + \frac{\partial \tau_{zr}}{\partial z} - \frac{\sigma_\theta}{r} = \frac{\partial p}{\partial r} \tag{21-a}$$

$$\frac{1}{r}\frac{\partial}{\partial r}(r\tau_{rz}) + \frac{\partial \sigma_z}{\partial z} = \frac{\partial p}{\partial z} \tag{21-b}$$

$$(\beta\lambda_w + \frac{\lambda_a}{P})\frac{\partial p}{\partial t} + \frac{\partial e}{\partial t} = (\frac{k}{\rho_w g})\nabla^2 p \tag{21-c}$$

It is very difficult to solve above obtained partial differential equations analytically. Here, we adopt the finite element method which has already been verified by authors of its applicability for plane strain state problem. In the following section the governing equations for axially symmetric problem are transformed into finite element equations.

3. FINITE ELEMENT FORMULATION

The Galerkin method[3),4),7)] which is one of the weighted residual methods is used to derive a finite element equations of the system of Eqs. (21). Now we put Eqs. (21) into following equations.

$$L_1(u_r, u_z, p) = \frac{1}{r}\frac{\partial}{\partial r}(r\sigma_r) + \frac{\partial \tau_{zr}}{\partial z} - \frac{\sigma_\theta}{r} - \frac{\partial p}{\partial r} = 0 \tag{22-a}$$

$$L_2(u_r, u_z, p) = \frac{1}{r}\frac{\partial}{\partial r}(r\tau_{rz}) + \frac{\partial \sigma_z}{\partial z} - \frac{\partial p}{\partial z} = 0 \tag{22-b}$$

$$L_3(u_r, u_z, p) = (\beta\lambda_w + \frac{\lambda_a}{P})\frac{\partial p}{\partial t} + \frac{\partial e}{\partial t} - (\frac{k}{\rho_w g})\nabla^2 p = 0 \tag{22-c}$$

In the finite element method the analytical region is divided into a set of sub-domains called element. The continuous functions u_r, u_z and p are approximated by following interpolation formulation over each sub-domain.

$$u_r = \sum_{j=1}^{n} a_j(t)\phi_j(r,z) \tag{23-a}$$

$$u_z = \sum_{j=1}^{n} b_j(t)\phi_j(r,z) \tag{23-b}$$

$$p = \sum_{j=1}^{n} c_j(t)\phi_j(r,z) \tag{23-c}$$

where, n is the number of node in each element. a_j, b_j and c_j are the nodal values of u_r, u_z and p respectively. ϕ_j is the shape functions dependent only on coordinates. Applying Galerkin method to Eqs. (22),

$$\int L_1(u_r, u_z, p)\,\phi_j dV = 0 \qquad (j = 1,2,\cdots,n) \tag{24-a}$$

$$\int L_2(u_r, u_z, p)\,\phi_j dV = 0 \qquad (j = 1,2,\cdots,n) \tag{24-b}$$

$$\int L_3(u_r, u_z, p)\,\phi_j dV = 0 \qquad (j = 1,2,\cdots,n) \tag{24-c}$$

where, $dV = 2\pi r dr dz$.
Substituting Eqs. (22) into Eqs. (24).

$$\int \frac{1}{r}\frac{\partial}{\partial r}(r\sigma_r)\phi_i 2\pi r dr dz + \int \frac{\partial}{\partial z}(\tau_{zr})\phi_i 2\pi r dr dz - \int \frac{\sigma_\theta}{r}\phi_i 2\pi r dr dz - \int \frac{\partial p}{\partial r}\phi_i 2\pi r dr dz = 0 \tag{25-a}$$

$$\int \frac{1}{r}\frac{\partial}{\partial r}(r\tau_{rz})\phi_i 2\pi r dr dz + \int \frac{\partial}{\partial z}(\sigma_z)\phi_i 2\pi r dr dz - \int \frac{\partial p}{\partial z}\phi_i 2\pi r dr dz = 0 \tag{25-b}$$

$$(\beta\lambda_w + \frac{\lambda_a}{P})\int \frac{\partial p}{\partial t}\phi_i 2\pi r dr dz + \int \frac{\partial e}{\partial t}\phi_i 2\pi r dr dz - \frac{k}{\rho g}\int \left\{\frac{1}{r}\frac{\partial}{\partial r}\left(r\frac{\partial p}{\partial r}\right) + \frac{\partial^2 p}{\partial z^2}\right\}\phi_i 2\pi r dr dz = 0 \tag{25-c}$$

Applying Green's theorem to the terms involving second order derivatives in r and z direction.

$$\int n_r r\sigma_r \phi_i 2\pi dz - \int r\sigma_r \frac{\partial \phi_i}{\partial r} 2\pi dr dz + \int n_z \tau_{zr}\phi_i 2\pi r dr - \int \tau_{zr}\frac{\partial \phi_i}{\partial z} 2\pi r dr dz - \int \frac{\sigma_\theta}{r}\phi_i 2\pi r dr dz - \int \frac{\partial p}{\partial r}\phi_i 2\pi r dr dz = 0 \tag{26-a}$$

$$\int n_r r\tau_{rz} \phi_i 2\pi dz - \int r\tau_{rz} \frac{\partial \phi_i}{\partial r} 2\pi dr dz + \int n_z \sigma_z \phi_i 2\pi r dr - \int \sigma_z \frac{\partial \phi_i}{\partial z} 2\pi r dr dz - \int \frac{\partial p}{\partial z}\phi_i 2\pi r dr dz = 0 \tag{26-b}$$

$$(\beta\lambda_w + \frac{\lambda_a}{P})\int \frac{\partial p}{\partial t}\phi_i 2\pi r dr dz + \int \frac{\partial e}{\partial t}\phi_i 2\pi r dr dz - \frac{k}{\rho g}\left\{\int n_r r \frac{\partial p}{\partial r}\phi_i 2\pi dz - \int r \frac{\partial p}{\partial r}\frac{\partial \phi_i}{\partial r} 2\pi dr dz + \int n_z \frac{\partial p}{\partial z}\phi_i 2\pi r dr - \int \frac{\partial p}{\partial z}\frac{\partial \phi_i}{\partial z} 2\pi r dr dz\right\} = 0 \qquad (26\text{-c})$$

where, n_x and n_z are direction cosines in x and z direction respectively. Substituting the stress-strain relationships (16), (17), (18) and interpolation formulations (23) into volumetric integration terms of above equations, following equations are obtained.

$$\sum_{j=1}^{n}\left[\left\{(\lambda'+2G)\int \frac{\partial \phi_j}{\partial r}\frac{\partial \phi_i}{\partial r}dV + \lambda'\int \frac{1}{r}\phi_j \frac{\partial \phi_i}{\partial r}dV + G\int \frac{\partial \phi_i}{\partial z}\frac{\partial \phi_j}{\partial z}dV + (\lambda'+2G)\int \frac{1}{r^2}\phi_j\phi_i dV + \lambda'\int \frac{1}{r}\frac{\partial \phi_j}{\partial r}\phi_i dV\right\}a_j + \left\{\lambda'\int \frac{\partial \phi_j}{\partial z}\frac{\partial \phi_i}{\partial r}dV + G\int \frac{\partial \phi_j}{\partial r}\frac{\partial \phi_i}{\partial z}dV + \lambda'\int \frac{1}{r}\frac{\partial \phi_j}{\partial z}\phi_i dV\right\}b_j + \left\{\int \frac{\partial \phi_j}{\partial r}\phi_i dV\right\}c_j\right] = \int (n_r\sigma_r + n_z\tau_{zr})\phi_i dS \qquad (27\text{-a})$$

$$\sum_{j=1}^{n}\left[\left\{G\int \frac{\partial \phi_j}{\partial z}\frac{\partial \phi_i}{\partial r}dV + \lambda'\int \frac{1}{r}\phi_j\frac{\partial \phi_i}{\partial z}dV + \lambda'\int \frac{\partial \phi_j}{\partial r}\frac{\partial \phi_i}{\partial z}dV\right\}a_j + \left\{G\int \frac{\partial \phi_j}{\partial r}\frac{\partial \phi_i}{\partial r}dV + (\lambda'+2G)\int \frac{\partial \phi_j}{\partial z}\frac{\partial \phi_i}{\partial z}dV\right\}b_j + \left\{\int \frac{\partial \phi_j}{\partial z}\phi_i dV\right\}c_j\right] = \int (n_r\tau_{rz} + n_z\sigma_z)\phi_i dS \qquad (27\text{-b})$$

$$\sum_{j=1}^{n}\left[\left\{\int \frac{\partial \phi_j}{\partial r}\phi_i dV + \int \frac{1}{r}\phi_i\phi_j dV\right\}\frac{\partial a_j}{\partial t} + \left\{\int \frac{\partial \phi_j}{\partial z}\phi_i dV\right\}\frac{\partial b_j}{\partial t} + \left\{\frac{k}{\rho g}\left(\int \frac{\partial \phi_j}{\partial r}\frac{\partial \phi_i}{\partial r}dV + \int \frac{\partial \phi_j}{\partial z}\frac{\partial \phi_i}{\partial z}dV\right)\right\}c_j + \left\{\left(\beta\lambda_w + \frac{\lambda_a}{P}\right)\int \phi_j\phi_i dV\right\}\frac{\partial c_j}{\partial t} = \frac{k}{\rho g}\int \left(n_r\frac{\partial p}{\partial r} + n_z\frac{\partial p}{\partial z}\right)\phi_i dS \qquad (27\text{-c})$$

A finite difference method is applied for the terms with respect to time. In general the finite difference formulations are as follows.

$$\frac{\partial f_j}{\partial t} = \frac{(f_j^{t+\Delta t} - f_j^t)}{\Delta t}, \qquad f_j = \theta f_j^{t+\Delta t} + (1-\theta)f_j^t \qquad (28)$$

where, θ=0 represents an explicit scheme, θ=1/2 represents a centered difference scheme (Crank Nicholson scheme) and θ=1 represents a fully implicit scheme in time. Using above relationship and introducing the matrix notation, Eqs. (27) become as follows.

$$\begin{bmatrix} \theta A_{ij} & \theta B_{ij} & \theta\rho g C_{ij} \\ \theta D_{ij} & \theta E_{ij} & \theta\rho g F_{ij} \\ \dfrac{1}{\Delta t}H_{ij} & \dfrac{1}{\Delta t}P_{ij} & \rho g\dfrac{\beta\lambda_w+\lambda_a/P}{\Delta t}Q_{ij}+\theta k R_{ij} \end{bmatrix}^{t+\Delta t} \begin{Bmatrix} a_j \\ b_j \\ c_j \end{Bmatrix} =$$

$$\begin{bmatrix} (\theta-1)A_{ij} & (\theta-1)B_{ij} & (\theta-1)\rho g C_{ij} \\ (\theta-1)D_{ij} & (\theta-1)E_{ij} & (\theta-1)\rho g F_{ij} \\ \dfrac{1}{\Delta t}H_{ij} & \dfrac{1}{\Delta t}P_{ij} & \rho g\dfrac{\beta\lambda_w+\lambda_a/P}{\Delta t}Q_{ij}+(\theta-1)k R_{ij} \end{bmatrix}^{t} \begin{Bmatrix} a_j \\ b_j \\ c_j \end{Bmatrix} + \begin{Bmatrix} F_i^{(1)} \\ F_i^{(2)} \\ F_i^{(3)} \end{Bmatrix} \tag{29}$$

where,

$$A_{ij} = (\lambda'+2G)\int \frac{\partial\phi_j}{\partial r}\frac{\partial\phi_i}{\partial r}dV + \lambda'\int \frac{1}{r}\phi_j\frac{\partial\phi_i}{\partial r}dV + G\int \frac{\partial\phi_i}{\partial z}\frac{\partial\phi_j}{\partial z}dV + (\lambda'+2G)\int \frac{1}{r^2}\phi_j\phi_i dV + \lambda'\int \frac{1}{r}\frac{\partial\phi_j}{\partial r}\phi_i dV \tag{29-a}$$

$$B_{ij} = \lambda'\int \frac{\partial\phi_j}{\partial z}\frac{\partial\phi_i}{\partial r}dV + G\int \frac{\partial\phi_j}{\partial r}\frac{\partial\phi_i}{\partial z}dV + \lambda'\int \frac{1}{r}\frac{\partial\phi_j}{\partial z}\phi_i dV \tag{29-b}$$

$$C_{ij} = \int \frac{\partial\phi_j}{\partial r}\phi_i dV \tag{29-c}$$

$$D_{ij} = G\int \frac{\partial\phi_j}{\partial z}\frac{\partial\phi_i}{\partial r}dV + \lambda'\int \frac{1}{r}\phi_j\frac{\partial\phi_i}{\partial z}dV + \lambda'\int \frac{\partial\phi_j}{\partial r}\frac{\partial\phi_i}{\partial z}dV \tag{29-d}$$

$$E_{ij} = G\int \frac{\partial\phi_j}{\partial r}\frac{\partial\phi_i}{\partial r}dV + (\lambda'+2G)\int \frac{\partial\phi_j}{\partial z}\frac{\partial\phi_i}{\partial z}dV \tag{29-e}$$

$$F_{ij} = \int \frac{\partial\phi_j}{\partial z}\phi_i dV \tag{29-f}$$

$$H_{ij} = \int \frac{\partial\phi_j}{\partial r}\phi_i dV + \int \frac{1}{r}\phi_i\phi_j dV \tag{29-g}$$

$$P_{ij} = \int \frac{\partial\phi_j}{\partial z}\phi_i dV \tag{29-h}$$

$$Q_{ij} = \int \phi_j\phi_i dV \tag{29-i}$$

$$R_{ij} = \int \frac{\partial\phi_j}{\partial r}\frac{\partial\phi_i}{\partial r}dV + \int \frac{\partial\phi_j}{\partial z}\frac{\partial\phi_i}{\partial z}dV \tag{29-j}$$

$$F_i^{(1)} = \int (n_r\sigma_r + n_z\tau_{zr})\phi_i dS \tag{29-k}$$

$$F_i^{(2)} = \int (n_r\tau_{rz} + n_z\sigma_z)\phi_i dS \tag{29-l}$$

$$F_i^{(3)} = \int \left(n_r\frac{\partial p}{\partial r} + n_z\frac{\partial p}{\partial z}\right)\phi_i dS \tag{29-m}$$

Eq.(28) is the element stiffness matrix for each sub-domain element. It is necessary to superpose the element stiffness matrices to create a global system of stiffness matrix. After that, we can solve a system of linear equations for each time step. In this study, we adopt $\theta = 1/2$ considering its stability in the calculation.

4. OUTLINE OF NUMERICAL ANALYSIS AND EXPERIMENT

4.1 Numerical Procedure

For the analysis, a simplified sand bed model as shown in Fig. 2 is treated. Considering the experimental conditions, we adopted following boundary conditions and numerical conditions.

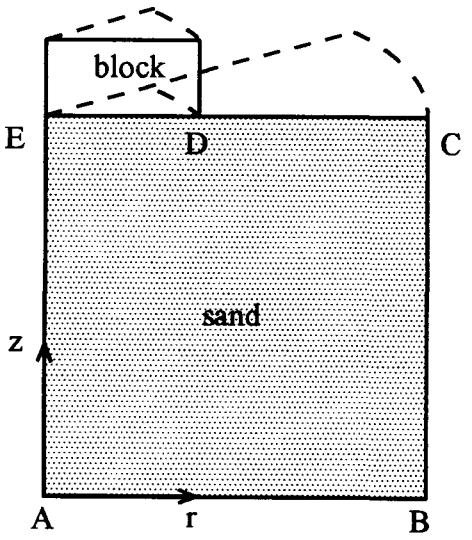

Fig. 2 Sand bed model in analysis

Boundary conditions :

(a) $h = h_s(t)$ at CD

(b) $\partial h / \partial n = 0$ at AB, BC, EA

(c) $n_r \sigma_r + n_z \tau_{zr} = 0$, $n_r \tau_{rz} + n_z \sigma_z = 0$ at CD

(d) load due to the pressure $h = h_s(t)$ acting the block at DE

where, $h_s(t)$ is the oscillating water pressure acting on the sand surface and the block.

Numerical conditions :

$\lambda_a = 0.005$, $\lambda_w = 0.4$, $k = 0.015(\mathrm{cm/s})$, $\beta = 4.3 \times 10^{-10}(\mathrm{m^2/N})$,

$G = 3.5 \times 10^7(\mathrm{N/m^2})$, $\nu = 0.45$

In this study we adopted triangular elements to divide the domain. Fig. 3 shows the finite element mesh. Its node number is 345 and element number is 623. In the calculation, at first, the initial stress state without the cyclic loading of water pressure is obtained by taking into account the individual weight of the block and the sand. After that, the incremental value due to cyclic loading of water pressure is added to the initial one.

4.2 Experimental Procedure

For the experiment the rectangular parallelepiped container shown in Fig. 4 was used. The width of the container is 40 cm. It is filled with highly saturated standard sand (Toyoura standard sand $d_{50} \cong 0.25$ mm). The water depth from the sand surface is about 110 cm. The oscillating

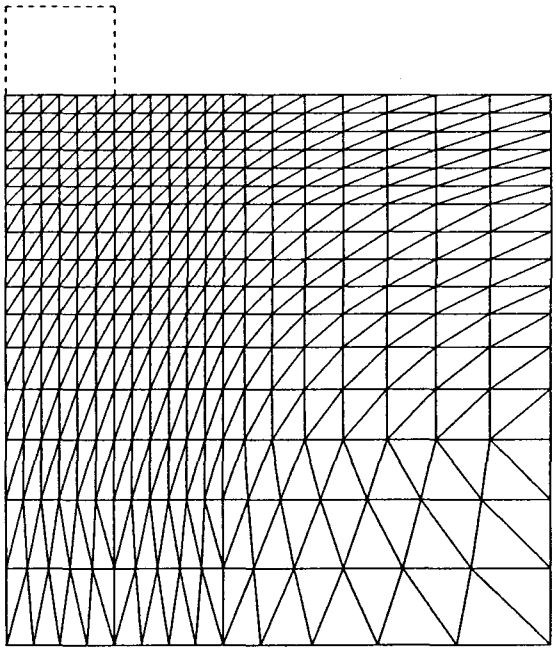

Fig. 3 Finite element mesh

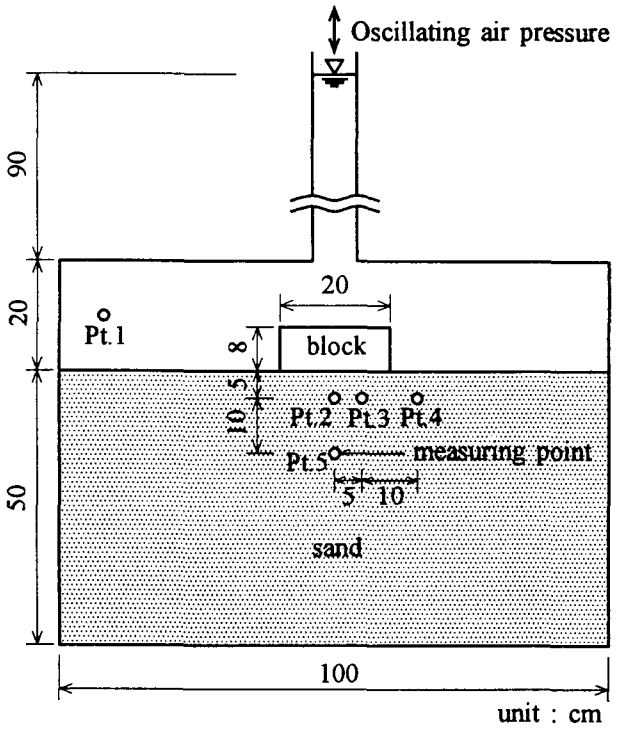

Fig. 4 Experimental apparatus

air pressure acts on the water surface. The amplitude of the cyclic water pressure acting on the sand surface is about 40 cm. Its frequency is about 1 Hz. A cylindrical block was placed at the center of the sand surface. Its diameter is 20 cm and its specific weight is 3.65. The incremental pore water pressure were measured at measuring points shown in Fig. 4.

5. RESULTS AND DISCUSSIONS

Fig. 5 (a) and (b) shows the numerical and experimental results of the pore water pressure variation at each measuring points. Experimental results show that the water pressure on the sand surface propagates into the sand bed accompanied by the damping in amplitude and the phase lag. This tendency is very similar to the results for the rectangular block[1),2)]. From the numerical analysis, the characteristics of the damping and the phase lag of the pore pressure around the block are in good agreement with experimental results. That is, the validity of the mathematical model and the numerical method developed in this paper can be verified.

Fig. 6. shows the distribution of the pore water pressure and the seepage force. Fig. 6 (a) is for the state that the water pressure on the sand surface is high (t/T=0.25), and Fig. 6 (b) is for the low pressure state(t/T=0.75). In this figure, solid lines show the equipotential lines and arrows show the seepage force vector. The pore water pressure propagates into the sand bed

around the block with the damping in amplitude and the phase lag cyclically. This pore water pressure variation around the block causes the cyclic seepage force around the block. This cyclic seepage force at the low water pressure state plays an very important role in the settlement of the block under the cyclic loading of water pressure[2].

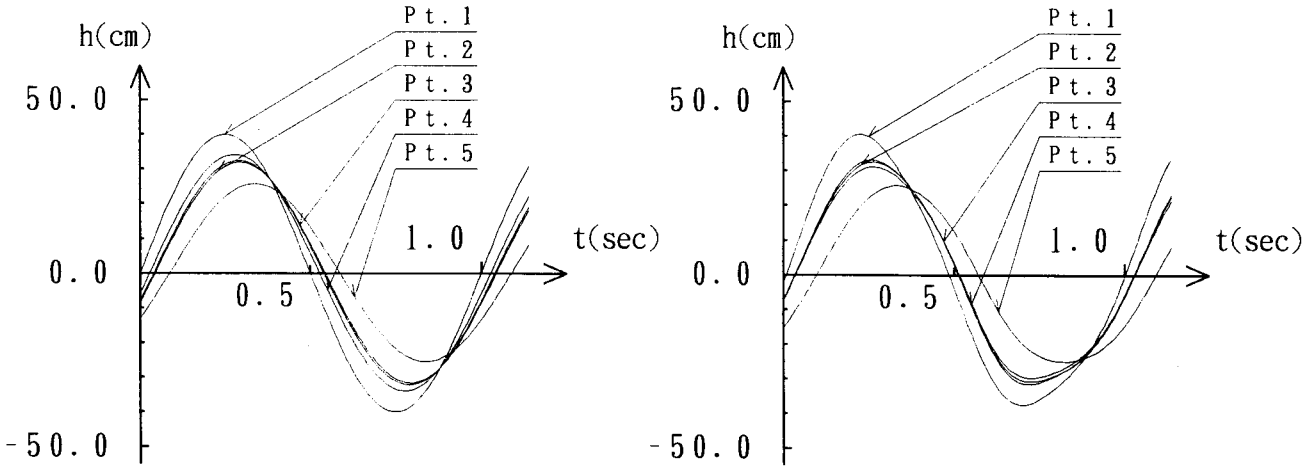

Fig. 5 Pore water pressure variation with time

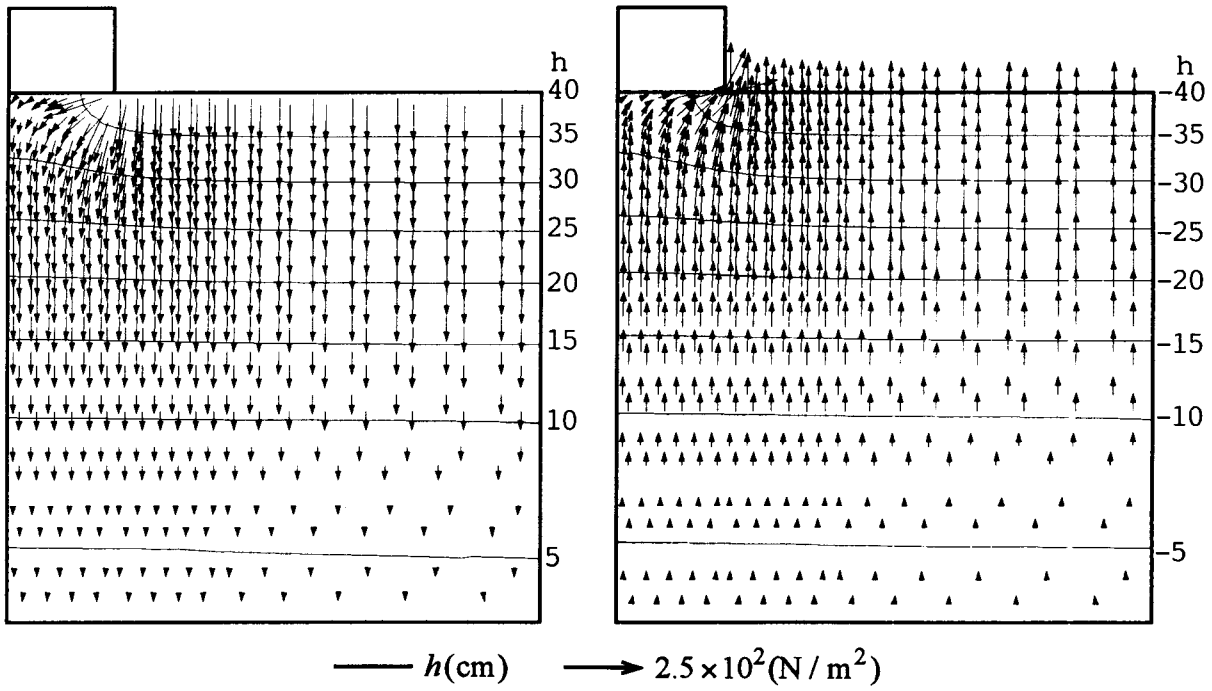

Fig. 6 Pore water pressure and seepage force

6. CONCLUSIONS

In this paper, we derived the fundamental equations to analyze the dynamic behavior of the sand bed around the cylindrical block under the cyclic loading of water pressure and evaluated the applicability of numerical method based on the derived mathematical model through the experiment. The numerical results by the finite element method showed the good agreement with experimental results. It can be concluded that the validity of the mathematical model and numerical method presented in this paper is verified.

REFERENCES

1) Maeno, S. and Nago, H. : Settlement of a concrete block into a sand bed under water pressure variation, Proceedings of the International Symposium on Modelling Soil-Water-Structure Interactions, pp. 67-76, 1988.

2) Nago, H. and Maeno, S. : Settlement of concrete block into sand bed under cyclic loading of water pressure, Proc. of 26th IAHR Congress, Vol. 3, pp. 317-322, 1995.

3) Nago, H. and Maeno, S. : Pore water pressure in sand bed under oscillating water pressure, Memoirs of the School of Engineering, Okayama Univ., Vol. 19, No. 1 pp. 13-32. 1984.

4) Nago, H., Maeno, S., Sasahara, H. and Nishioka, M. : Prevention work of the settlement of coastal block, Proceedings of Civil Engineering in the Ocean, Vol. 6, pp. 229-234, 1990, (in Japanese).

5) Verruijt, A. : Elastic storage of aquifers, Flow Through Porous Media, Ed. DeWiest, R. J. M., Academic Press, New York, pp. 337-344, 1969.

6) Timoshenko, S. and Goodier, J. N. : Theory of elasticity, Second Edition, McGraw-Hill Book Company, Inc., New York, pp. 304-306, 1951.

7) Szabo, B. A. and Lee, G. C. : Derivation of stiffness matrices for problems in plane elasticity by Galerkin's method, International Journal of Numerical Methods in Eng. Vol. 1, pp. 301-310, 1969.